Original Article

JSA

J Strain Analysis
47(4) 203–213

DOI: 10.1177/0309324712441433
sdj.sagepub.com
SAGE

Residual stress characterization in 12%-Cr steel friction stir welds by neutron diffraction

Tea-Sung Jun[1], Felix Hofmann[2], Michael Hofmann[3] and Alexander M Korsunsky[2]

Abstract

In the present paper we report the results of a study into friction stir welds made in 12.7 mm-thick 12%-Cr steel plates. Residual stress measurements were performed using angle-dispersive neutron diffraction. Complete characterization of the three-dimensional residual stress state in friction stir weld samples was obtained by analysing diffracted peaks; peak broadening for identifying the regions of severe plastic deformation and the associated residual strain (eigenstrain) acting as the source of residual stress and peak shifting for evaluating residual elastic strains in the welded component. Three different methods were used to address the key issue of determining the d_0 variation across the weld. The *comb* (or matchstick) method was compared with two other approaches: the *balance* method, and the *zero traction* method. It was found that a combination of the comb and the zero traction methods allows reliable residual strain/stress distributions.

Keywords

Friction stir welding, residual stress, full-width at half-maximum, neutron diffraction

Date received: 26 October 2011; accepted: 9 February 2012

Introduction

Among the manufacturing processes that cause residual stresses in engineering components, welding is one of the most significant. Although welding is necessary to join the components, it frequently leaves behind tensile residual stresses that are likely to have adverse effects on structural integrity. Conventional fusion welding, in general, produces large tensile stresses with a maximum value that is approximately equal to the yield strength of the materials being joined, balanced by lower compressive residual stresses elsewhere in the component. Much attention has been paid to the reduction, or at least to control of the magnitude of these stresses due to the fact that tensile residual stresses may promote cracking and failure of manufactured components, and reduce their durability.

Recently, friction stir welding (FSW) has been introduced as a solid state joining process that involves no attendant melting. Not only may the residual stresses created by the welding process be considerably reduced by FSW, but also other properties such as microstructure, fatigue life, tensile strength, etc. can significantly improved compared with conventional welding techniques.

Friction stir welding was first proposed and patented around 1991 at TWI (The Welding Institute, UK) and is built on a remarkably simple concept. The welding process uses a welding tool which consists of a shoulder and a pin. The tool is rotated around its axis and inserted at the interface between the abutting edges of the two plates or sheets being joined, that are simultaneously being pressed together in a jig. The tool then translates along the interface, and 'zips' it together.[1–3] The tool serves two primary functions such as (a) heating of the workpiece, and (b) stirring and intermingling of the material(s) to produce the joint. The heat is generated by the friction between the tool and the workpiece. The localized heating softens the material around the pin, and the combination of tool rotation and translation leads to the movement of material from the front

[1]Welding and Joining Research Group, POSCO, South Korea
[2]Department of Engineering Science, University of Oxford, UK
[3]FRM II, TU München, Germany

Corresponding author:
Tea-Sung Jun, Welding and Joining Research Group, POSCO, Pohang, Gyeongbuk, 790-300, South Korea.
Email: terryjun83@gmail.com

of the pin to the back of the pin. During the FSW process, the material undergoes intense plastic deformation at elevated temperature, resulting in the generation of fine and equiaxed recrystallized grains at some locations.[4–8]

The process creates asymmetric structures in the welded plates due to the addition and subtraction between the tool rotation speed and the tool travel speed that occur to two sides of the pin path, called the advancing and retreating sides, respectively. The former may receive a somewhat higher heat input than the latter due to the higher relative velocity of the tool,[9] resulting in different microstructure and mechanical properties. In general, the advancing side has higher tensile properties and hardness.[10–13] As an effect of the friction stir welding process, four different forms of microstructure are observed in the welded plates. Parent material (PM) which exists relatively far from bond line shows no material deformation during the FSW process. Remote material is affected by neither the heat flux nor in terms of the microstructure and mechanical properties. In the weld nugget (WN), the original grain structure appears to be replaced with fine, equiaxed recrystallized grains characterized by the nominal dimension of a few μm. The material in the thermal-mechanically affected zone (TMAZ) is plastically deformed by the tool in the presence of the high heat flux and considerably elevated temperature. This exerts some influence on the material microstructure, and as a consequence extensive deformation is evident in this zone. The heat affected zone (HAZ) is a zone where the material has undergone a thermal cycle that modified the microstructure and/or mechanical properties. However, no plastic deformation occurred in this area.[4,5] Note here sometimes the term weld zone (WZ) is used to refer to the combined region of WN and TMAZ.

So far a number of studies have been conducted on FSW in order to identify and verify the advantages of friction stir welding compared with conventional welding processes, such as arc welding, laser welding, electron beam welding, etc. The practical suitability of this joining method is also being investigated for many industries, such as aerospace, automobile manufacture, ship building, etc. Most studies, however, have focused on light (e.g. aluminium) alloys,[14–22] while the application to the materials with higher melting temperatures, such as steel and titanium, has been limited by the difficulty of identifying suitable welding tool materials. Polycrystalline cubic boron nitride (PCBN) and alloys based on tungsten-rhenium (W-25Re) have been the leading candidates. However, neither material has so far fulfilled all of the requirements for a friction stir weld tool material, such as the sufficient resistance to wear and thermal loading, and toughness.[23–25] In spite of the tool wear, the mechanical properties of FSW joints of steel components are usually found to be acceptable. However, very limited data is available on the residual stress states.[26,27]

Recently, FSW of steel plates has been successfully carried out using refractory metal welding tools at TWI. It is noted from the macro-structural appearance of the weld sections (see Figure 1) that great improvements have been achieved in terms of low porosity and low number of bonding defects.[28] In particular aspects of steel-FSW, the phase in WZ is in general hardened during welding process due to the phase transformation governed by cooling rate, chemical composition, grain size, etc. For the use of this technique in industrial applications, improved understanding of the residual stresses is necessary so as to account for their presence in design calculations, and to control them during deformation or thermal processing. The present study aims to investigate the effect of mechanical and thermal behaviour of FSW process in these improved FSW joints between thick (about ½ inch) 12%-Cr steel plates.

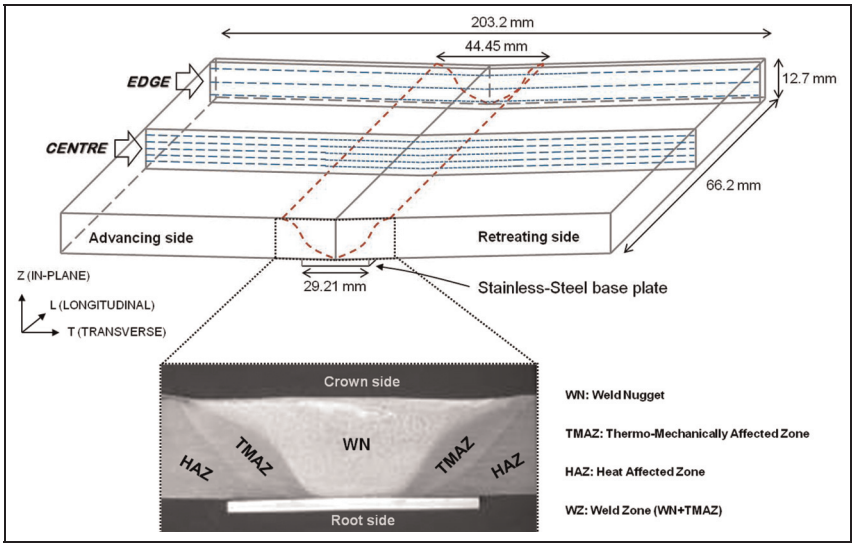

Figure 1. Schematic diagram and macro-structure in the 12% Cr FSW weld.

In this paper, residual strain measurements in FSW welds by means of neutron diffraction are presented and analysed. One of the key problems arising in the residual strain analysis of weld joints is the problem of determining the variation of the unstrained (reference) lattice parameter as a function of position with respect to the FSW joint. In the present study, three different options have been considered for obtaining the variation of the unstrained lattice spacing, d_0. The results for the residual strains/stresses are then discussed in comparison with the corresponding full-width at half-maximum (FWHM) and hardness measurements.

Experimental

Specimen preparation

The material used in the present study was a 12%-Cr alloy steel, with the chemical composition (in wt %): Cr – 10.5~12.5, Mn – 1.5, Ni – 0.3~1.0, C – 0.03, N – 0.030, P – 0.04, S – 0.015, Si – 1.0, Fe balance. The welds were manufactured at TWI (The Welding Institute, Abington, Cambridge, UK) by butt welding two chromium steel plates, with the refractory metal welding tools. The tool geometry and dimension were substantially that of Whorl^{TM} type as described elsewhere (e.g. in Mishra and Ma[3]) and 45 mm shoulder diameter with 10~14 mm probe diameter base-tip, respectively. The plates were placed on a stainless steel base plate to protecting the machine bed. In the process, the down-force was fixed at 32 kN, rotational speed fixed at 625 r/min, lateral speed fixed at 2mm/sec. The specification of the welds is shown in Figure 1. The dimensions of the welds were $203.2 \times 66.2 \times 12.7$ mm^3, cut from the centre region in the initial welds of $203.2 \times 1000 \times 12.7$mm^3. Note that residual stresses were relaxed after cutting but assume that the effect was minor. Temperature history during the process was measured using thermal imaging measurements.[29] It is shown in Figure 2 that a maximum temperature close to the tool was approximately 1000 °C. It should be noted here that the phase in WZ over the course of thermal cycle is simply estimated by Schaeffler diagram,[30] such that the phase transformation would be ferrite to austenite during welding, and to ferrite plus martensite during cooling. Near the EDGE region (see Figure 1), a 3 mm slice was machined by EDM (electrical discharge machining), for the purpose of making a 'comb' sample.

Residual strain measurements

Residual strain measurements on the welds were conducted by neutron diffraction at STRESS-SPEC, FRM-II facility in Garching, Germany (TU München) with a constant neutron wavelength of $\lambda = 1.6638$ Å. Neutron diffraction is particularly well suited to residual strain determination in dense materials in comparison, for example, with synchrotron radiation sources, since neutron absorption is less sensitive to the atomic number, and thus permits experiments involving longer beam paths. The key area of interest in this investigation was the cross-section (T–Z plane) at the CENTRE and EDGE of the weld. Before carrying out the measurements, the outline profile of the welds was measured using CMM (Coordinate Measuring Machine) at Oxford HEXLab, in order to improve the experimental accuracy during diffraction measurement. As can be seen in Figure 3, the contour was then plotted in Matlab and a grid of points spaced by 2 mm near the weld zone (±40 mm from the bond line) and ±4 mm across the weld zone was superimposed to identify the locations of the centres of measurement gauge volumes.

Figure 4 shows the experimental set-up with the identification of the main components: incident beam slits, sample stages, detector, etc. A two-dimensional (2D) position-sensitive[3] He detector (PSD), a multi-wire detector with delay time encoding and with the active area of 200×200 mm^2, was used to collect the diffraction patterns. The sample was aligned on the translation stage such that the measurement reference frame coincided with the system of axes assigned in Matlab. Thus, the centroid of each gauge volume could be accurately lined up with the corresponding measurement node.

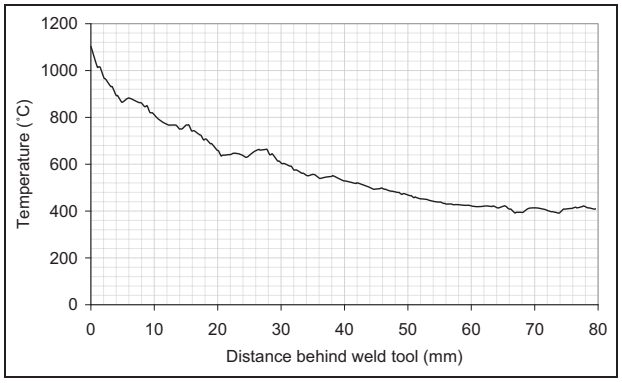

Figure 2. Temperature history of the 12% Cr steel welds.

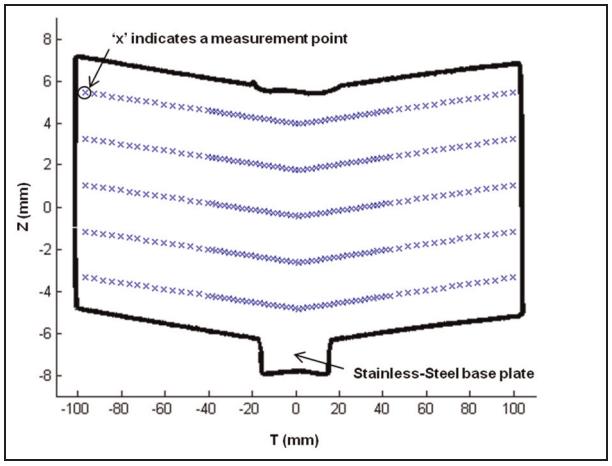

Figure 3. CMM outline image of the welds.

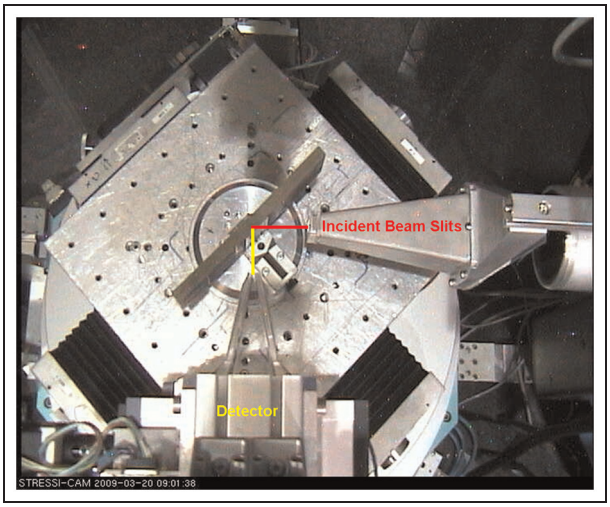

Figure 4. Experimental set-up at stress-spec.

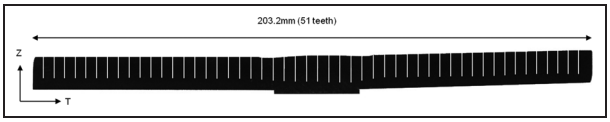

Figure 5. Comb sample for the determination of strain-free reference values.

For the measurement of lattice spacing in steel, the (2 1 1) reflection was used as it is generally recommended in literature for the evaluation of macrostrains in α-Fe lattices.[31] This is due to the good peak intensity and its relative insensitivity to plastic strain effects. Since the possibility of using relatively large gauge volumes provides good averaging and produces smoother maps, gauge volume of $2 \times 2 \times 2\,\text{mm}^3$ and counting time for each measurement point of 120 s were used for the whole experiment. Diffraction patterns were collapsed into line profiles, and peak centre positions determined by fitting, allowing the shifts of the Bragg peak centres $\Delta\theta$ to be determined.[32]

For the 'strain-free' or unstrained lattice parameter d_0, the 'comb' sample was machined by EDM (see Figure 5). Note that the *comb* method is effective when making teeth parallel to the welding direction for a weldment, since no steep variation in d_0 is expected in that direction.[33,34] Fifty-one teeth, 4 mm wide (T-direction) and 8mm long (z-direction) were cut from the sample slice of 4 mm thickness (L-direction), with a basic assumption that the stress field in the T- and L-directions is totally relaxed by the cutting process. The measurements were made at mid-length in the teeth with the same experimental set-up as above. However, note that only measurements in transverse direction were made due to the lack of experimental time.

Hardness testing

For the hardness contour map, Vickers hardness tests were conducted on the same region (T-Z plane) as the strain measurement using a diamond pyramid indenter. The loading mass of 30 kg was used, and the dimensions of the indents were measured by optical microscope to determine hardness. The result was represented as a hardness contour map.

Results

Analysis of the unstrained lattice parameter

It has been much discussed in the literature and is well-known that in some respects obtaining the correct unstrained lattice parameter is the most crucial part of any residual strain measurement by diffraction.[33] Note that it is particularly difficult to determine this parameter in a welded structure. This is due to the fact that the welding process creates inhomogeneous thermal and mechanical fields, leading to the plastic deformation being accompanied by recrystallization and hence a change of microstructure and probably a re-distribution of chemical composition due to carbide precipitation in the structure.[34,35] In the present study, three different approaches to obtaining the unstrained lattice parameter variation were employed to determine the residual strains and hence stresses.

Option 1: The comb method. Due to the limitation of the 'comb' measurement, it was assumed that the unstrained lattice parameters in the transverse, in-plane and longitudinal directions are identical. Figure 6(a) shows the distribution of the lattice parameter. The

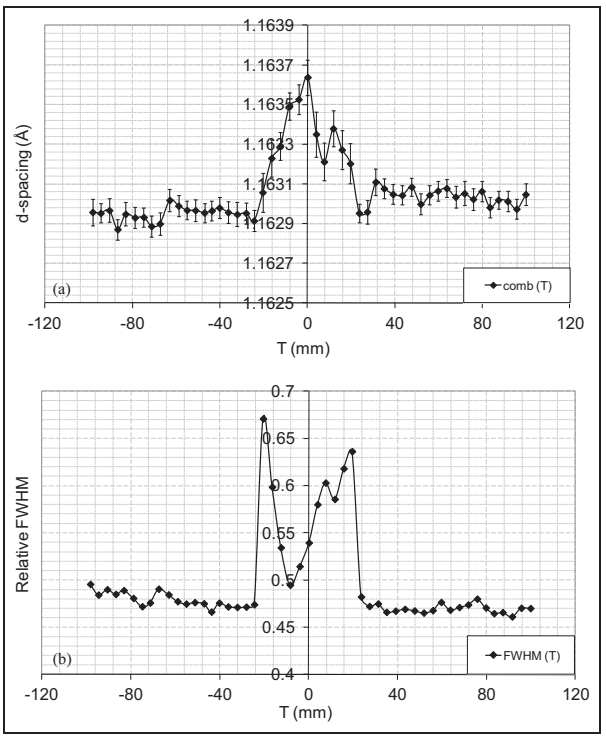

Figure 6. Distribution of (a) unstrained lattice parameter in the transverse direction, (b) FWHM in the transverse direction. FWHM: full-width at half-maximum.

lattice parameter changes significantly in the weld zone (within about ±22 mm from the bond line) that corresponds to the diameter of the shoulder of the welding tool. Outside this zone the observed variation was insignificant. This means that the welds were plastically deformed mainly by the rotating shoulder, induced by high temperature and mechanical pressure. Regions associated with plastic deformation can clearly be seen in Figure 6(b) that shows the increased peak-width values in the weld zone.[36]

Option 2: The balance method. Obtaining the unstrained lattice parameter by averaging the entire stress field in a certain direction and applying global shift correction is only valid if no spatial variation in d_0 exists and the macrostress is directly coupled to the d_0 shift. This method is to adopt the fundamental continuum mechanics requirements that are stress balance and strain compatibility. Ensure that the experimental data set covers the entire cross section and not just a part of it.[34] In this method, a global value of a_0 was obtained instead of d_0 (so that correction could be applied to all peaks), leading to the determination of the so-called nominal strains. The typical nominal strain error of 50×10^{-6} was obtained, corresponding to stress uncertainty of only about 10 MPa for steel.

Option 3: The zero traction method. In order to achieve - improvement over the *comb* method that only provided measurements of the unstrained lattice parameter in the transverse direction, the so-called *zero traction* method was also proposed in the present study. The purpose of the analysis was to determine the variation of the unstrained lattice parameter in the longitudinal direction. The fundamental hypothesis of the zero traction method is this: since the stress field in L-direction was totally relieved by the cutting process, it was assumed that the longitudinal stresses in the region just below the T–Z plane at the EDGE of the weld must be equal to zero *at each point of the weld*. From the triaxial Hooke's law, the longitudinal stresses along the transverse direction can be written down as follows

$$\langle \sigma_L \rangle_Z = \frac{\mathrm{E}}{(1+\nu)(1-2\nu)} \left[(1-\nu)\left(\frac{d^L - d_0^L}{d_0^L} \right) + \nu(\varepsilon_T + \varepsilon_Z) \right] \quad (1)$$

Then, the unstrained lattice parameter in the longitudinal direction d_0^L was sought under the condition $\langle \sigma_L \rangle_Z = 0$. Figure 7 shows the distribution of d_0^L reconstructed by the *zero traction* method. Note that the unstrained lattice parameter in the longitudinal direction also varies in the weld zone as does in the transverse direction (see Figure 6(a)), and was applied to calculate the longitudinal residual strains.

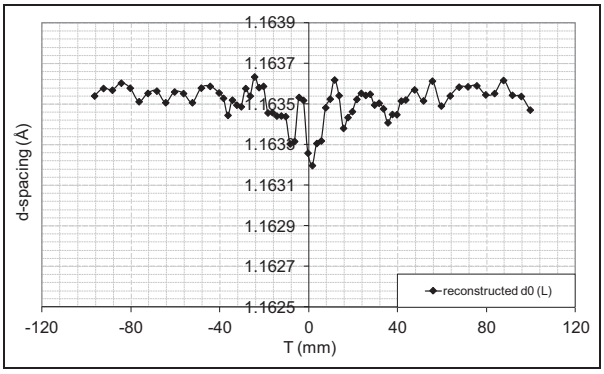

Figure 7. Distribution of reconstructed unstrained lattice parameter in the longitudinal direction.

Averaged lattice spacing

Before applying the three options for the determination of unstrained lattice parameter, the lattice spacing is presented in Figure 8 in order to visualize the nature of the distribution. Figure 8 shows the distributions of the averaged lattice spacing at the EDGE and CENTRE sections of the welds, respectively. The traction in the longitudinal direction was completely relieved by the EDM cutting process. The resulting interpretation demonstrates significant lattice spacing variation across the EDGE section of the weld. It is argued here that this result is justified by the physical, metallurgical and mechanical considerations: the complex thermo-mechanical processes occurring during welding cause solute migration, phase changes and hence result in

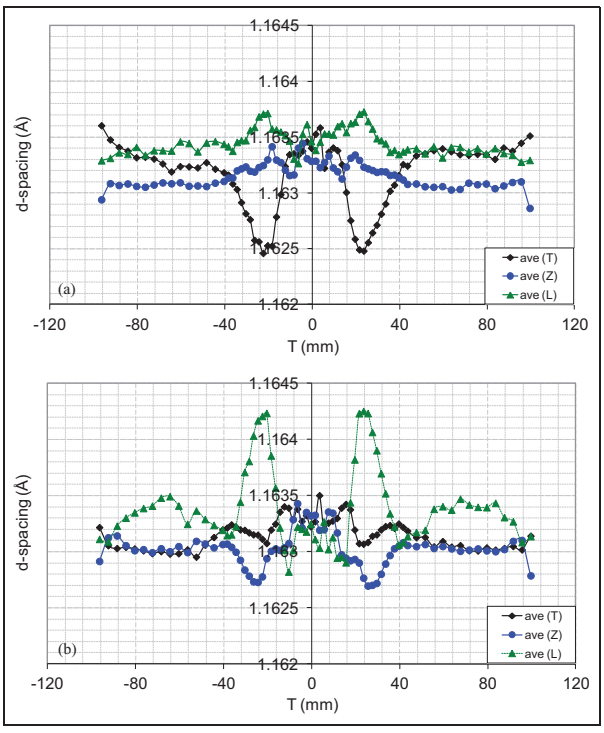

Figure 8. Distribution of averaged lattice spacing at (a) EDGE and (b) CENTRE of the welds.

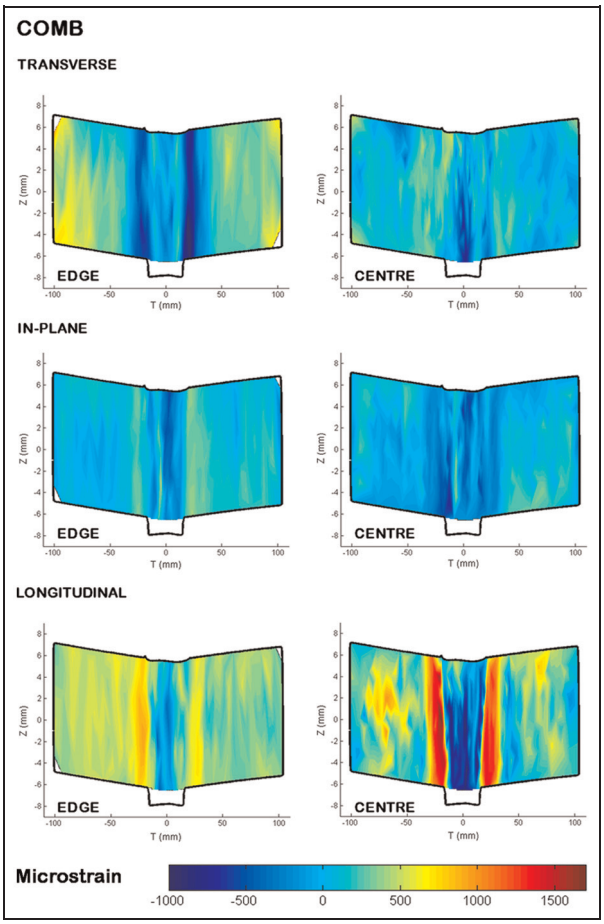

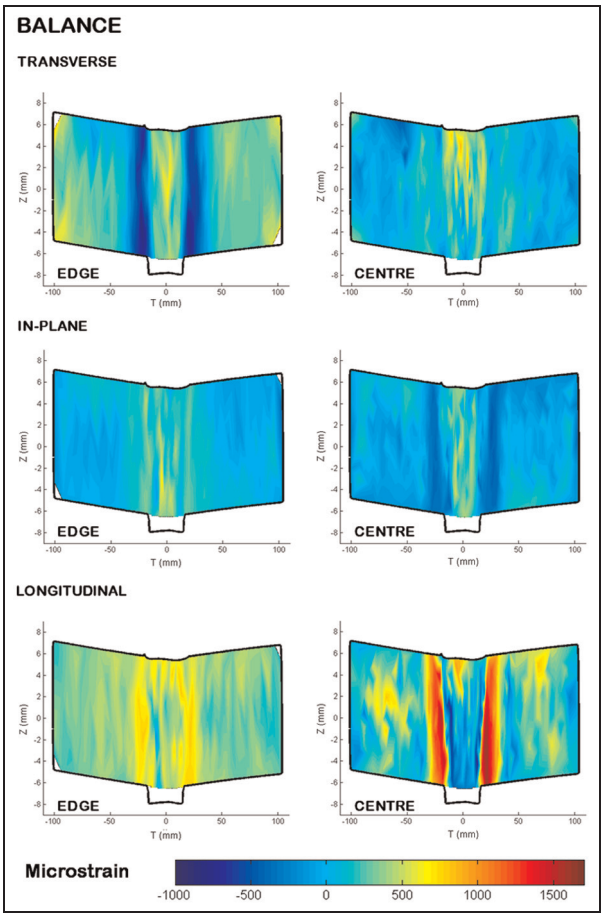

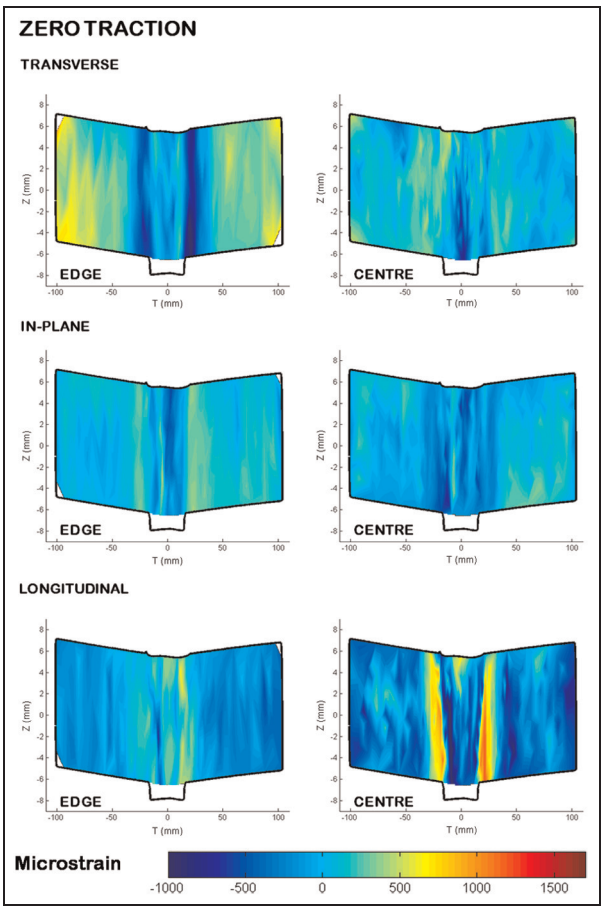

Figure 9. Distribution of residual elastic strains at EDGE and CENTRE of the weld with three options.

lattice spacing variation. At the same time, the mechanics considerations require that the out-of-plane traction on a free surface must vanish, and this requirement is enforced by the *zero traction* analysis.

Residual elastic strains

The residual elastic strains were calculated on the basis of the three options used for the determination of the unstrained lattice parameter. Figure 9 shows the contour plot of the strains in the EDGE and CENTRE of the weld. The results can be summarized as follows.

(a) In the *comb* method, significant strain variations can be found in the longitudinal direction at the CENTRE region. Unlike in the conventional fusion welding, compressive strains are found in the weld zone and tensile strains in the heat affected zone, as a consequence of the friction stir welding process.[9] This may be caused by phase transformation from austenite to martensite during cooling immediately after welding, resulting in the volume increase in the zone. There are no significant strain variations in the transverse and in-plane directions, apart from existing compressive

strains at minor regions in the weld nugget for the former direction and in the weld nugget and the heat affected zone for the latter. At the EDGE region, relieved strains can be seen in the longitudinal direction.

(b) In the *balance* method, it can be clearly seen that the three-directional (3D) strain distributions at the EDGE and CENTRE regions are considerably similar as those in *comb* method, except in the weld zone. Compared with *comb* method, the nominal strain error outside the weld zone is about 100×10^{-6}, corresponding to the stress uncertainty of only about 20 MPa for steel. On the other hand, the one in the weld zone is about 1000×10^{-6}, and 200 MPa as a stress uncertainty.

(c) In the *zero traction* method, the longitudinal strains were obtained using the reconstructed unstrained lattice parameter whilst the other strains were the same as those in *comb* method. Compared with the *comb* method, a small level of longitudinal strain at the CENTRE region was found in the weld and heat affected zone. On the other hand, tensile strains found outside the heat affected zone become compressive if this method is used.

(d) Asymmetric longitudinal strain distributions at CENTRE region were found in a small region below the crown side. This is probably associated with the asymmetric deformation during the welding process.

Validation of residual strain measurement

In order to validate the strain measurement, high resolution energy-dispersive X-ray diffraction was used to measure the centre line at the CENTRE region, on beamline ID15 at the European Synchrotron Radiation Facility (ESRF) in Grenoble, France.[37] Twin detector set-up was used to allow simultaneous measurement of strain parallel (L-direction) and perpendicular (T-direction) to the weld. Both detectors were mounted at fixed scattering angles of $2\theta = 5°$. The middle line in-plane (Z-direction) was chosen to measure with beam spot size of $0.5 \times 0.5\,\text{mm}^2$ and counting time of 20 s per point. The obtained data were analysed by single peak fitting of the (2 1 1) reflection and GSAS (general structure analysis system[38]) using Pawley refinement. For the unstrained lattice parameter, the *balance* method was used to determine the residual strains. Figure 10 shows the comparison of the transverse and longitudinal strains obtained using the *balance* method by neutron and synchrotron X-ray diffraction. It is found that both diffraction methods agree well, apart from a small discrepancy in the weld and heat affected zone.

Residual stresses

The strain data obtained were used to calculate the residual stresses using Hooke's law for triaxial stress, i.e.

$$\sigma_T = \frac{E}{(1+\nu)(1-2\nu)}[(1-\nu)\varepsilon_T + \nu(\varepsilon_L + \varepsilon_Z)] \quad (2a)$$

$$\sigma_L = \frac{E}{(1+\nu)(1-2\nu)}[(1-\nu)\varepsilon_L + \nu(\varepsilon_Z + \varepsilon_T)] \quad (2b)$$

$$\sigma_Z = \frac{E}{(1+\nu)(1-2\nu)}[(1-\nu)\varepsilon_Z + \nu(\varepsilon_T + \varepsilon_L)] \quad (2c)$$

where $E = 200$ GPa and $\nu = 0.3$. Figure 11 shows the contour plot of the stresses in the EDGE and CENTRE of the welds. The results can be summarized as follows.

(a) In the *comb* method, it is seen in the longitudinal direction at CENTRE region that significant compressive and tensile residual stresses exist in the weld and heat affected zone, respectively. In the same region, the distributions of transverse and in-plane stresses are close to each other, such that small levels of compressive stresses are found mainly in the weld nugget, whilst tensile stresses exist in the heat affected zone. At EDGE region, it is interesting to note that considerable tensile stresses were found outside the weld zone in the longitudinal direction, although no or low stress was expected due to stress relaxation. Therefore, it is thought and recommended that measuring and applying the *comb* method in all directions of strain measurements is imperative to obtain accurate values of macrostrain or macrostress.

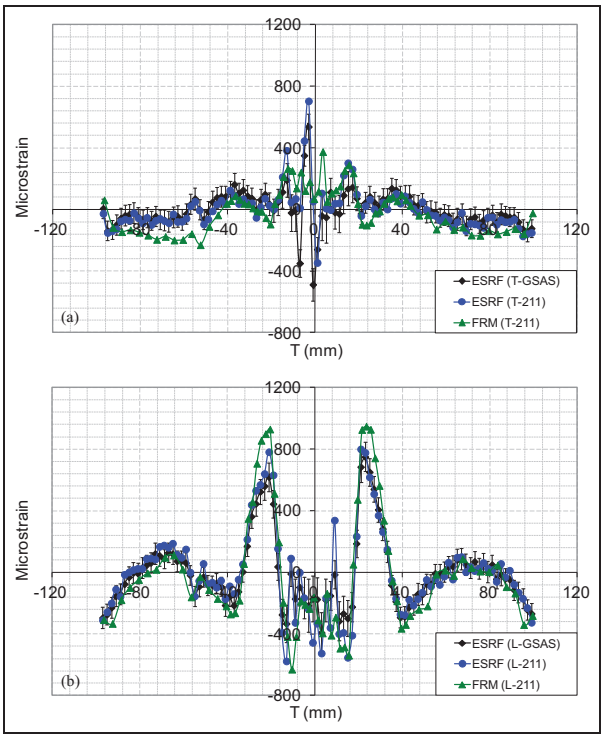

Figure 10. Distribution of averaged elastic strains using balance method in (a) transverse and (b) longitudinal direction at MID of the weld. ESRF: European Synchrotron Radiation Facility; FWHM: full-width at half-maximum.

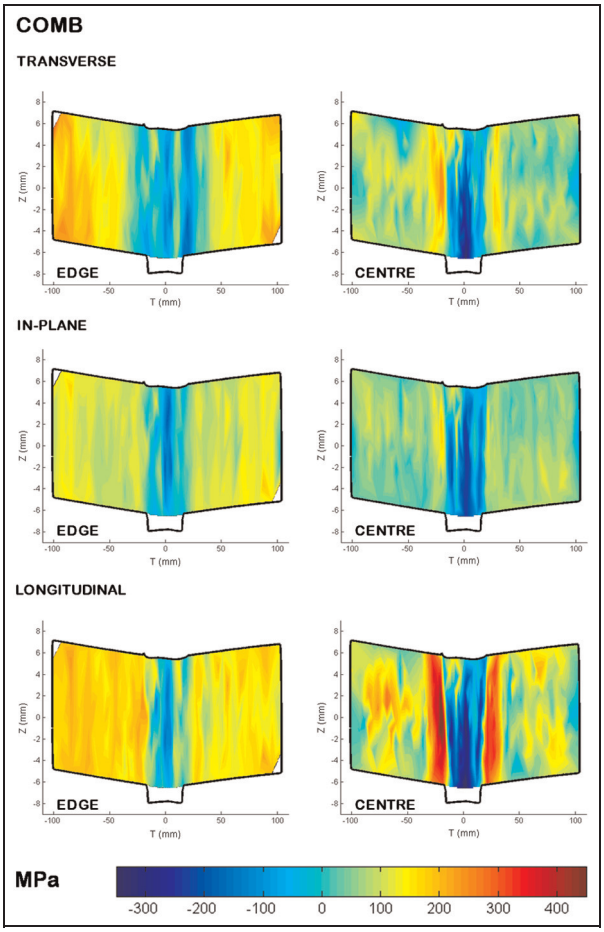

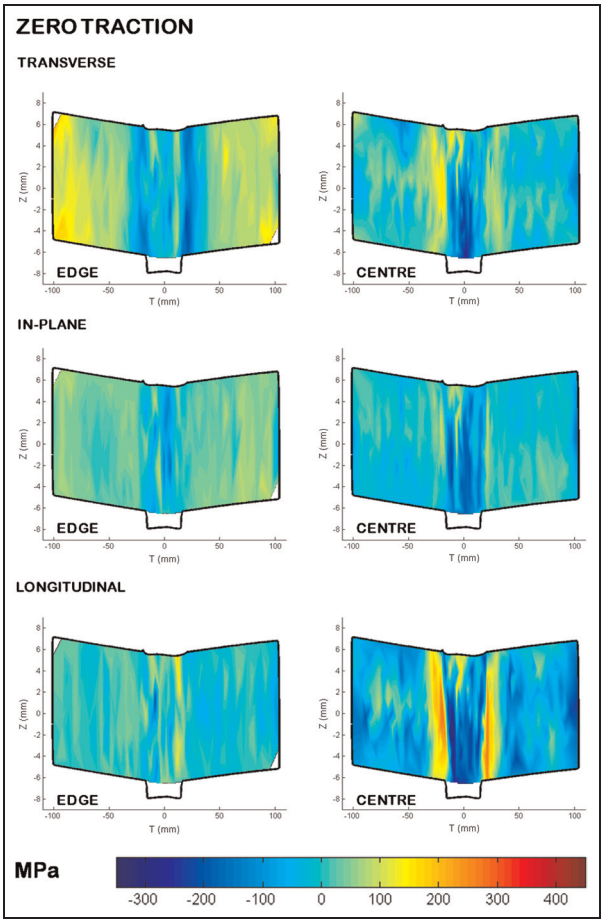

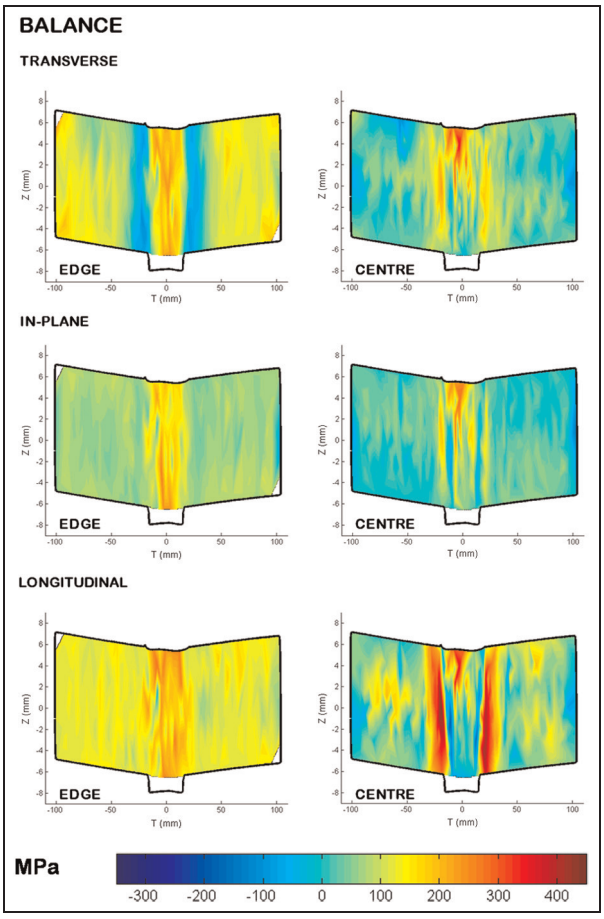

Figure 11. Distribution of residual stress at EDGE and CENTRE of the welds.

(b) In the *balance* method, the difference in the stress variations compared with the *comb* method was mainly observed in the weld zone.

(c) In the *zero traction* method, no or low stress was found at the EDGE region, particularly in the longitudinal direction where the effect of stress relaxation was directly accounted for. At the EDGE region, compressive and tensile stresses were distributed in the weld and heat affected zone, respectively, whereas no or low stress outside the zone was seen, unlike in the *comb* method. No significant stress variations were found in the transverse and in-plane direction, apart from the weld nugget where the compressive stresses were concentrated.

FWHM

It is well known that, while diffraction peak position is related to the average elastic strain or so-called macro-strain within the scattering grains, the diffraction peak shape is related to crystallite size and the so-called micro-strain, which refers to the spread of the lattice parameter values around the average. The spread or broadening is caused by the inhomogeneity of

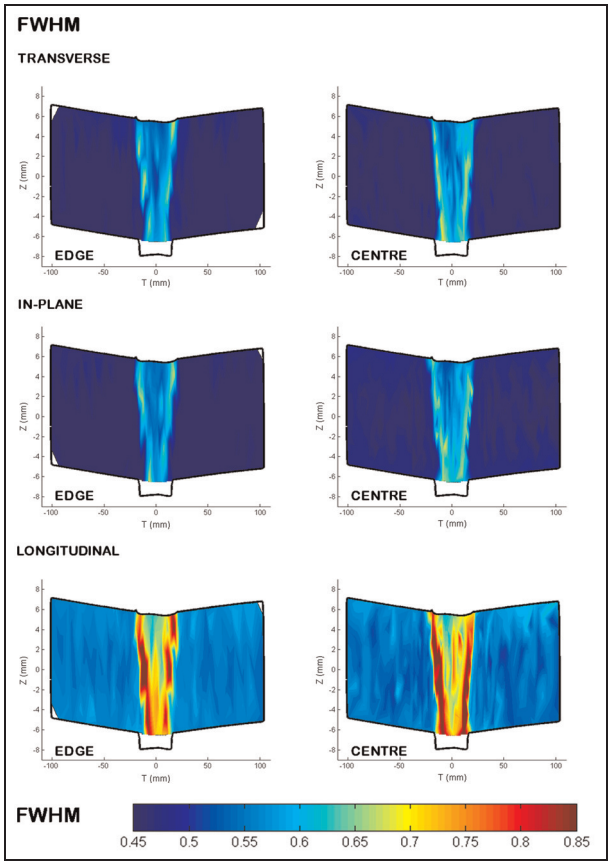

Figure 12. Distribution of FWHM at EDGE and CENTRE of the welds. FWHM: full-width at half-maximum.

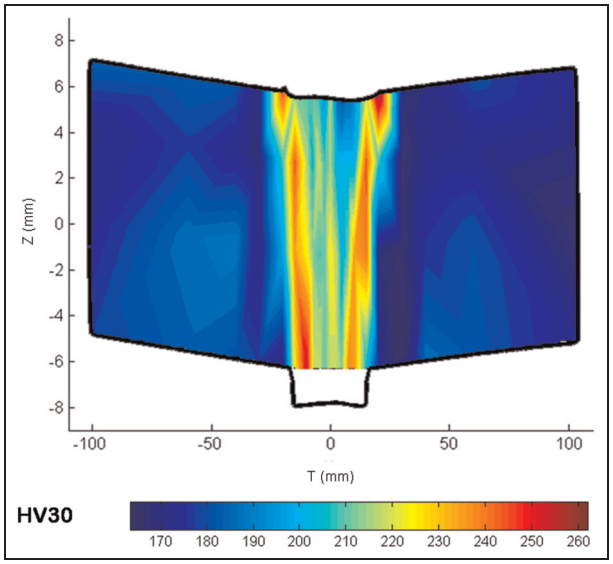

Figure 13. Distribution of hardness on the welds.

deformation between scattering grains and also within each grain as a consequence of dislocation density evolution, which in turn is related to plastic strain. Therefore, the variation of FWHM within the sample can be the basis for the choice of the size of region exposed to eigenstrains.[39] Figure 12 shows the contour plot of the FWHM in the EDGE and CENTRE of the welds. It can clearly be seen that the plastic deformation is localized in the weld zone at both EDGE and CENTRE regions. Interestingly, the more severe plastic deformation can be found in the thermo-mechanically affected zone, specifically the region corresponding to the edge of the pin. It may be surmised that in the weld nugget dynamic recrystallization occurred. One possibility of explaining this effect can be associated with the local deformation caused by the welding tool in the TMAZ. It is known that friction stir welding process introduces severe microstructure change in terms of grain size, structure and orientation at the interface between weld nugget and TMAZ.[6] This change may be sufficient to induce significant dislocation density and sub-grain formation, but not enough to recrystallize and/or recover the grains to a significant degree.[40]

In addition, it is interesting and important to note that the distribution of FWHM including that in 'comb' measurement (see Figure 6(b)) supports the theory of eigenstrain. The eigenstrain indicates any permanent strain arising in the material due to some inelastic process such as plastic deformation, crystallographic transformation, thermal expansion mismatch between different parts of an assembly, etc. It thus accounts for all permanent strains that arise in the material exhibiting inelastic behaviour. Based on the distribution of elastic strains and FWHM, the eigenstrain distribution can be determined using inverse eigenstrain method.[41] Consequently, the entire full-field 2D or 3D residual stress state can be reconstructed at every point within the structure. The work on eigenstrain analysis will be published in a separate paper.

Hardness

Figure 13 shows the contour plot of the hardness of the welds. It is seen that the distribution of the hardness correlated considerably with that of the FWHM. In the weld zone, the material is harder than outside the zone, and this is related to the phase transformation and grain refinement. As can be seen in Figure 2, the temperature in the weld zone was reached above 1000 °C, partially changing the phase structure of steel from austenite to martensite.

Conclusion

The study described in this paper was devoted to the analysis of residual strains and stresses in 12%-Cr steel friction stir welds using angle-dispersive neutron diffraction. Complete characterization of the 3D residual stress state was obtained with the use of three different methods (i.e. the *comb* method, the *balance* method, and the zero traction method) for the determination of the variation. It was found that a combination of the comb and the *zero traction* methods allows reliable residual strain/stress distributions. Based on the analysis of

peak broadening and peak shift, residual elastic strains were found with identifying a region of severe plastic deformation. These results were also related to micro hardness measurements, in that highest hardness was found in the thermo-mechanically affected zone, where the most severe plastic deformation occurred. The computed residual stresses indicated that in the longitudinal direction there were compressive residual stresses present in the weld zone, whilst tensile stresses in the heat affected zone. Note that this observation has an opposite trend compared with general assumption that the welding process usually introduces a longitudinal tensile stress in the weld zone and compressive in the heat affected zone. This is probably as a consequence of phase transformations from austenite to martensite during cooling immediately after welding, resulting in the volume increase in the zone. In the transverse and in-plane directions, no significant stress variations were observed.

Funding

This research received no specific grant from any funding agency in the public, commercial or not-for-profit sectors.

Acknowledgements

The authors are grateful to the FRM II (STRESS-SPEC) for the provision of beamtime under the project no. 2463.

References

1. Deqing W, Shuhua L and Zhaoxia C. Study of friction stir welding of aluminum. *J Mater Sci* 2004; 39: 1689–1693.
2. Jun TS, Zhang SY, Golshan M, et al. Synchrotron energy-dispersive X-ray diffraction analysis of residual strains around friction welds between dissimilar aluminium and nickel alloys. *Mater Sci Forum* 2008; 571–572: 407–412.
3. Mishra RS and Ma ZY. Friction stir welding and processing. *Mater Sci Engng* R-Reports 2005; 50: 1–78.
4. Barcellona A, Buffa G, Fratini L, et al. On microstructural phenomena occurring in friction stir welding of aluminium alloys. *J Mater Process Technol* 2006; 177: 340–343.
5. Fratini L, Buffa G, Palmeri D, et al. Material flow in FSW of AA7075-T6 butt joints: Continuous dynamic recrystallization phenomena. *J Engng Mater Technol Trans ASME* 2006; 128: 428–435.
6. Jata KV and Semiatin SL. Continuous dynamic recrystallization during friction stir welding of high strength aluminum alloys. *Scripta Mater* 2000; 43: 743–749.
7. Liu G, Murr LE, Niou CS, et al. Microstructural aspects of the friction-stir welding of 6061-T6 aluminum. *Scripta Mater* 1997; 37: 355–361.
8. Rhodes CG, Mahoney MW, Bingel WH, et al. Effects of friction stir welding on microstructure of 7075 aluminum. *Scripta Mater* 1997; 36: 69–75.
9. Prime MB, Gnaupel-Herold T, Baumann JA, et al. Residual stress measurements in a thick, dissimilar aluminum alloy friction stir weld. *Acta Mater* 2006; 54: 4013–4021.
10. Buffa G, Donati L, Fratini L, et al. Solid state bonding in extrusion and FSW: Process mechanics and analogies. *J Mater Process Technol* 2006; 177: 344–347.
11. Liu HJ, Fujii H, Maeda M, et al. Tensile properties and fracture locations of friction-stir-welded joints of 2017-T351 aluminum alloy. *J Mater Process Technol* 2003; 142: 692–696.
12. Watanabe T, Takayama H and Yanagisawa A. Joining of aluminum alloy to steel by friction stir welding. *J Mater Process Technol* 2006; 178: 342–349.
13. Yan JH, Sutton MA and Reynolds AP. Notch tensile response of mini-regions in AA2024 and AA2524 friction stir welds. *Mater Sci Engng A-Struct Mater Properties Microstruct and Process* 2006; 427: 289–300.
14. Bussu G and Irving PE. The role of residual stress and heat affected zone properties on fatigue crack propagation in friction stir welded 2024-T351 aluminium joints. *Int J Fatigue* 2006; 25: 77–88.
15. Fratini L and Zuccarello B. An analysis of through-thickness residual stresses in aluminium FSW butt joints. *Int J Machine Tools Mf* 2006; 46: 611–619.
16. James MN, Hughes DJ, Hattingh DG, et al. Synchrotron diffraction measurement of residual stresses in friction stir welded 5383-H321 aluminium butt joints and their modification by fatigue cycling. *Fatigue Fract Engng Mater Structs* 2004; 27: 187–202.
17. John R, Jata KV and Sadananda K. Residual stress effects on near-threshold fatigue crack growth in friction stir welds in aerospace alloys. *Int J Fatigue* 2003; 25: 939–948.
18. Li Y, Murr LE and McClure JC. Flow visualization and residual microstructures associated with the friction-stir welding of 2024 aluminum to 6061 aluminum. *Mater Sci Engng A-Strucl Mater Properties Microstructure and Process* 1999; 271: 213–223.
19. Peel M, Steuwer A, Preuss M, et al. Microstructure, mechanical properties and residual stresses as a function of welding speed in aluminium AA5083 friction stir welds. *Acta Mater* 2003; 51: 4791–4801.
20. Staron P, Koçak M and Williams S. Residual stresses in friction stir welded Al sheets. *Appl Phys A* 2002; 74: S1161–S1162.
21. Staron P, Koçak M, Williams S, et al. Residual stress in friction stir-welded Al sheets. *Physica B* 2004; 350: e491–e493.
22. Sutton MA, Reynolds AP, Wang DQ, et al. A study of residual stresses and microstructure in 2024-T3 aluminum friction stir butt welds. *J Engng Mater Technol Trans ASME* 2002; 124: 215–221.
23. Fujii H, Cui L, Tsuji N, et al. Friction stir welding of carbon steels. *Mater Sci Engng A Struct Mater Properties Microstr Process* 2006; 429: 50–57.
24. Jones RL *Developments in joining processes for structural steel applications*. Cambridge: TWI, 1991.
25. Threadgill PL and Johnson R. *Progress in friction stir welding of steels*. Cambridge: TWI, 2004.
26. Reynolds AP, Tang W, Gnaupel-Herold T, et al. Structure, properties, and residual stress of 304L stainless steel friction stir welds. *Scripta Mater* 2003; 48: 1289–1294.
27. Barnes SJ, Steuwer A, Mahawish S, et al. Residual strains and microstructure development in single and sequential double sided friction stir welds in RQT-701 steel. *Mater Sci Engng A* 2008; 492(1-2): 35–44.

28. Tuck JR, Rowe CED, Thomas W, et al. *Refractory metal tooling for friction stir welding of hard aluminium and steel*. Cambridge: TWI, 2006.
29. Thomas WM, Threadgill PL and Nicholas ED. Feasibility of friction stir welding steel. *Sci Technol Welding Joining* 1999; 4: 365–372.
30. Schaeffler AL. Constitution diagram for stainless steel weld metal. *Metal Prog* 1949; 56(11): 680–680B.
31. Reimers W, Pyzalla AR, Schreyer A, et al. *Neutrons and synchrotron radiation in engineering materials science*. Wiley-VCH, 2008.
32. Hofmann M, Seidl GA, Rebelo-Kornmeier J, et al. The new materials science diffractometer STRESS-SPEC at FRM-II. *Resid Stresses Vii* 2006; 524–525: 211–216.
33. Hughes DJ, James MN, Hattingh DG, et al. The use of combs for evaluation of strain-free references of residual strain measurements by neutron and synchrotron X-ray diffraction. *J Neutron Res* 2003; 11: 289–293.
34. Withers PJ, Preuss M, Steuwer A, et al. Methods for obtaining the strain-free lattice parameter when using diffraction to determine residual stress. *J Appl Crystallography* 2007; 40: 891–904.
35. Woo W, Choo H, Brown DW, et al. Angular distortion and through-thickness residual stress distribution in the friction stir processed 6061-T6 aluminum alloy. *Mater Sci Engng A* 2006; 437(1): 64–69.
36. Tang CC, Lynch PA, Cheary RW, et al. An in situ method for the study of strain broadening using synchrotron X-ray diffraction. *J Appl Crystallography* 2007; 40: 642–649.
37. Luckhoo HT, Jun TS and Korsunsky AM. Inverse eigenstrain analysis of residual stresses in friction stir welds. *Procedia Engng* 2009; 1: 213–216.
38. Larson AC and Von Dreele RB. *General structure analysis system (GSAS) manual*. Los Alamos, NM: Los Alamos National Laboratory, 2004.
39. Jun TS and Korsunsky AM. Evaluation of residual stresses and strains using the Eigenstrain Reconstruction Method. *Int J Solids Structs* 2010; 45(13): 1678–1686.
40. Steuwer A, Peel MJ and Withers PJ. Dissimilar friction stir welds in AA5083-AA6082: The effect of process parameters on residual stress. *Mater Sci Engng A – Struct Mater Properties Microstruct Process* 2006; 441: 187–196.
41. Korsunsky AM, Regino GM and Nowell D. Variational eigenstrain analysis of residual stresses in a welded plate. *Int J Solids Structs* 2007; 44: 4574–4591.